Correlating Airborne Hyperspectral Images with Geological Field Data at Red Lake Ontario

Patrick Assouad*
Canada Centre for Remote Sensing
Natural Resources Canada
(613) 943-8821
Patrick.Assouad@ccrs.nrcan.gc.ca

Vern Singhroy
Canada Centre for Remote Sensing
Natural Resources Canada
(613) 947-1215
Vern.Singhroy@ccrs.nrcan.gc.ca

Abstract

A hyperspectral airborne campaign using the TRWIS sensor was undertaken in August 2001 in Red Lake, Ontario, to study the feasibility of using hyperspectral data as a tool for identifying small mineralized outcrops. In this paper, the methodology and results of correlating airborne and lab spectra are presented for the Marcus site location covered by the survey. Special emphasis is placed on the data post-processing needed for sensor corrections. Our results show that the distribution mapping of some alterations related to gold mineralization on the Marcus site in Red Lake can be made. However not all units were successfully identified from the airborne data.

Introduction

In the Red Lake greenstone belt of northern Ontario outcrops are generally less than 10 percent. Research needs to be conducted on the exposed bedrock to characterize their reflectance spectra from field and airborne techniques. The Red Lake greenstone belt is an important gold camp that has produced approximately 18.4 million ounces of gold by 1999. The majority of the gold deposits occur in an assemblage of pillowed, tholeiitic, basalt flows, basaltic komatite and spinifex-textured komatite flows interlayered with minor clastic metasedimentary and chert- magnetite iron formation. [1]. In this paper, we focus on the Marcus site which is located in the basaltic flows and consists mostly of phyllitic and propylitic altered rocks.

Data Acquisition

In August 2001, an aerial survey using the TRWIS III sensor was flown over the Red Lake greenstone belt with the aim of studying the application of hyperspectral technology to assist mapping and exploration in this type of setting. Field work for this particular site was conducted with the assistance of Goldcorp and Rubicon. Table 1 details the parameters of the survey over the study site presented here.

Table 1. Flight parameters for the Marcus site.

Acquisition Date	August 19, 2002
Acquisition Time GMT	15:46:00
Lat/Long	51.08/-93.78
Pixel Resolution	5 m.
Visibility	40 km
Tilt	0 (Nadir)

TRWIS III Sensor

The airborne TRW Imaging Spectrometer III (TRWIS III) sensor was developed and characterized by the TRW Space and Electronics Group as a predecessor to the Hyperion sensor launched by NASA on its EO-1 spacecraft. TRWIS III is a pushbroom sensor that records information on 384 contiguous bands in the 400 nm to 2450 nm range[2]. Two spectrometers are actually used to cover this range. The first covers the Visible/Near Infrared (VNIR) range between 370 nm and 1040 nm in 5.25 nm wide bands. The second covers the Short Wave Infrared (SWIR) from 890 nm to 2450 nm in 6.25 nm wide bands. The two spectrometers are co-aligned and matched in the crosstrack field of view to allow the co-registration of all bands. On readout, the instrument results in 256 pixel sampling in the crosstrack field of view which can range from 0.5 m to 11 m in resolution depending on the aircraft's altitude.

* Under contract to the Canada Centre for Remote Sensing from ACG Space Inc, Longueuil, Quebec

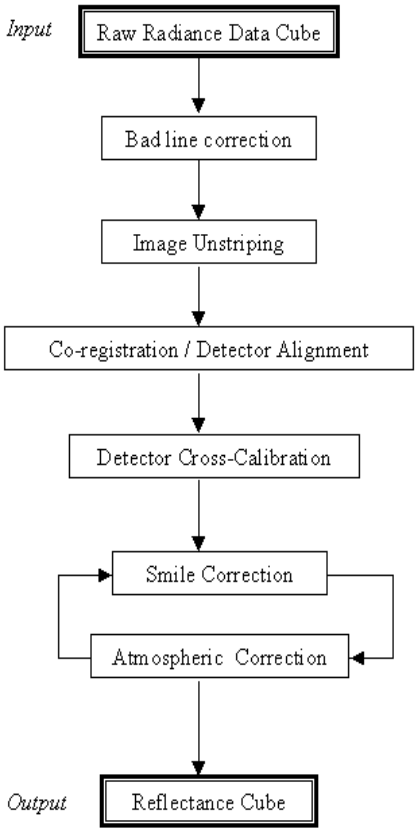

Figure 1. Schematic layout of the processing steps undertaken to extract a reflectance cube from the raw radiance data.

Figure 2. An RGB (bands 641, 551, 461, respectively) color composite of the area surrounding the study site. Bad row values and some vertical striping effects are seen.

Processing of Radiance Data

Figure 1 outlines the processing followed to transform the radiance spectral cube into an atmospherically corrected reflectance cube which can be used in association with ground and lab sample spectra. The following details each processing step. All correction steps were performed in the ISDAS environment developed at the Canada Centre for Remote Sensing, Natural Resources Canada [3].

Bad Line Corrections

Figure 2 shows an RGB colour composite of the raw radiance data around the study site. Some bad rows values are evident. These were simply removed by setting those values to equal the average radiance values of the two pixels in the nearest lines.

Data Unstriping

Figure 2 also displays some vertical striping effect along the crosstrack field of view. Two procedures were attempted to compensate for this, Fourier transforms and a crosstrack running average window. It was found that the Fast Fourier Transforms can provide good results but filters would have to be custom designed for each band image to assure that no residual effect is still present in spectra of the inverted result. This is a very time consuming proposition. A running average window (of one pixel size on either side of the averaged pixel) showed a decrease in striping without significant alteration of the radiance spectra and results from this process were used in subsequent analysis.

Detector co-registration

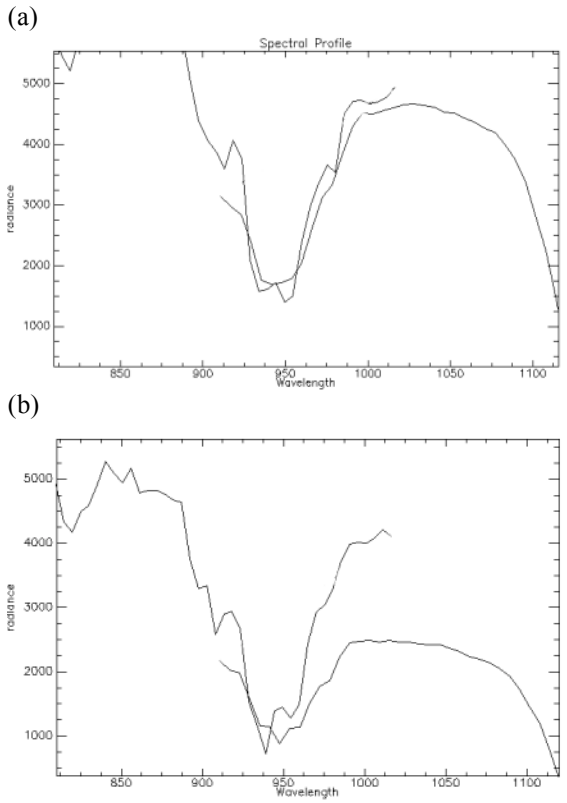

Figure 3. Example radiance spectra showing detectors band overlap (radiance units are $W/m^2/\mu m/sr$). Spectra (b) is representative of the largest offset observed in the data over the outcrop.

Analysis of the images from the VNIR and SWIR bands revealed that the sensor co-registration was not properly calibrated, resulting in a spatial shift (or distortion) between images from both detectors.

As first step, this distortion was corrected through a new module created within the ISDAS environment designed for this purpose [4]. Essentially, the user inputs linear displacement and rotation angle assumed for the offset between detectors. The choice is then made to resample either VNIR or SWIR detectors to match the other. Through an iterative approach and visual assessment, the best value for the input parameters can be found.

Detector cross-calibration

The spectral range of the detectors provides an overlap region in the 900 nm to 1000 nm range. This overlap allows for the evaluation of cross-calibration between detectors. Figure 3 shows this overlap in 2 pixels chosen to represent the extent of the offset variation. This offset is not constant as a function of pixel position and is hence very difficult to correct. No satisfactory result was obtained by trying to estimate gain and offset correction parameters. Another possible solution here is to resample the values of one detector to the band centers of the other and then average both radiance values. However, given the relatively small magnitude of the offset around the minimum of the 940 nm water feature, and the uncertainty in the behaviour of the VNIR sensor in its last bands, it was decided for the purposes of a preliminary analysis to only select values of the water feature from the SWIR, ignoring those of the VNIR. This allowed for a better continuity in spectral shape. In addition, this water feature will eventually serve to evaluate the water vapour content of each pixel for which the feature around 1400 nm is also used.

Smile Correction

The crosstrack spectral error, or "smile", is caused by distortion of the monochromatic image of the spectrometer slit onto the focal plane and by the rotation of the rows of focal plane pixels relative to the slit or grating [5]. This results in a slightly non-constant bandcentre for each band along the crosstrack pixels.

Presence of smile may cause difficulties in transforming the radiance data into reflectance through atmospheric correction. Incorrect bandcentres will result in an erroneous estimation of the water vapour content, under or over evaluating it, which will lead to artificial spikes in the reflectance spectra [4].

A module was created in ISDAS to compensate for this error. Essentially, the shifts in bandcentres are evaluated through iterative atmospheric corrections. Once the smile correction is performed, ISDAS outputs a hyperspectral reflectance cube.

Lab Spectral Measurements

Rock samples were collected across the study site and selected to represent each class of mineral alteration found. Fifteen samples were collected for this purpose. Spectral measurements were acquired using the ASD FieldSpec Pro spectrometer and referenced to a Spectralon panel. A more complete discussion of this technique is found in [6].

Figure 4 plots the spectral response of each main alteration class found on the study site as indicated by the collected samples.

Ground Data – Maps

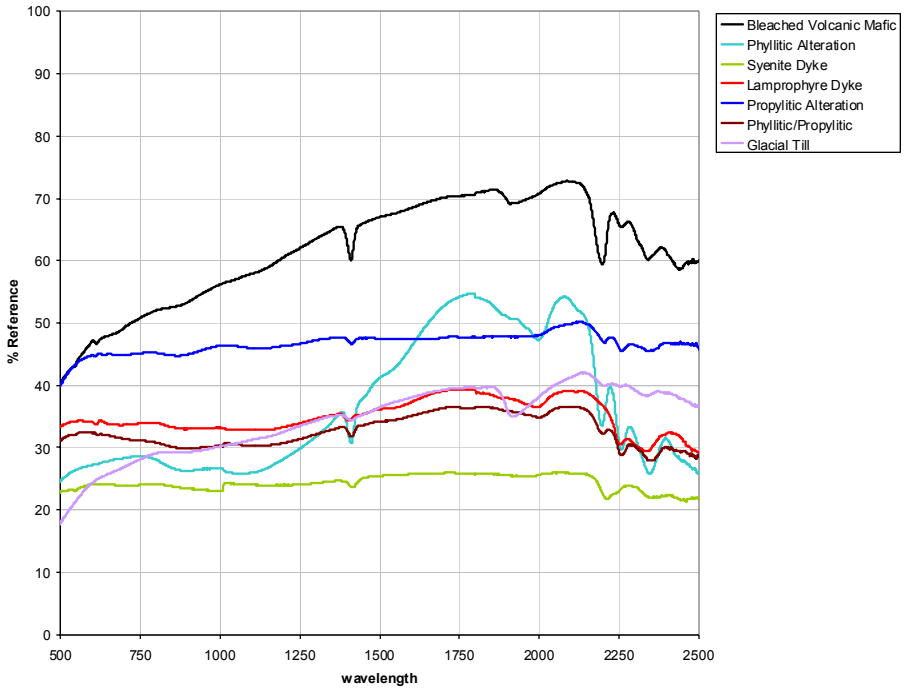

Figure 4. Spectral plot of the major constituent mineral alterations found on the Marcus Study site.

Detailed confidential geological maps at a scale of 1: 200 of the study site were provided by Goldcorp for validation of our results. Results of the correlations presented here are based on these maps.

Linear Unmixing Methodology

In this phase of the study, a partially constrained linear spectral mixing model is assumed whereby the resulting spectra of one pixel is simply the linear combination, or weighted average sum, of the proposed end-members [7]. The feasibility constraint applied to the model is that the end-member fraction coefficient must sum to unity.

The model follows the matrix equation:

$$P = EA + \Phi$$

where E is an M x N matrix, in which the columns are the end-member vectors in spectral space, A is a 1 x M matrix with unknown coefficient, P is a 1 x N vector representing the known pixel spectrum, and Φ is a 1 x N matrix with residuals. The equation is inverted to evaluate the A matrix and thus the fraction content of each end-member. Further feasibility constraints can be added to the system of equations where the coefficients must sum to unity and be non-negative.

This model has the advantage of simplicity, both conceptually and in the interpretation of the results. Processing is also straightforward and does not require much computational time. However, there are also drawbacks. The sum-to-unity constraint implies that all end-members are well known and that the spectra used for the analysis are representative of them. Modifying the end-member spectra by either altering the depth of some features, or simply removing (or adding) one end-member to the analysis can dramatically modify the resulting fraction coefficients.

Results

Figure 5 shows the results of the linear unmixing performed on 4 sections of the site. The sample spectra in figure 4 were used, over the 2000 nm to 2350 nm where most unique features appear, to map out their respective alteration. It was found that in virtually all pixels of the phyllitic alteration mentioned below, the pixel end-member actually matched better with the sample spectra of the phyllitic alteration overprinted by a propylitic alteration (shown in figure 4 as phyllitic/propylitic*). For this reason, only this sample spectra was used in the mapping process and all pixels were classified as phyllitic.*

Section 1

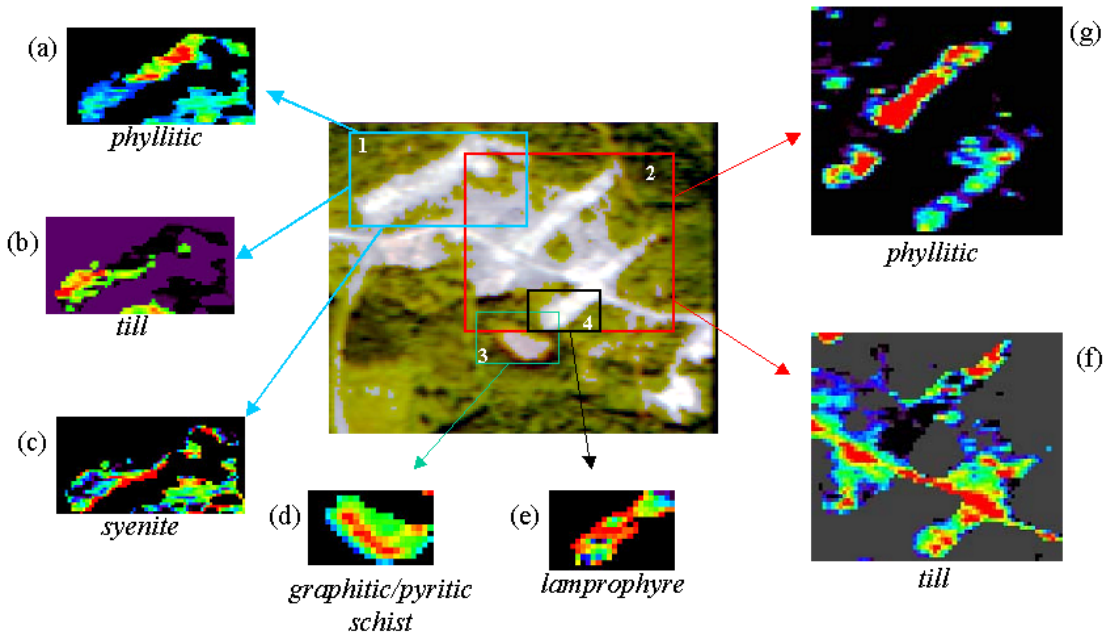

Figure 5. Mapping of end-member through various sections of the Marcus site. Red indicates higher fraction content, green and yellows are medium, blue is low.

The northwestern part of the site is composed mainly of a phyllitic alteration of the mafic volcanic rock. There is also a linear syenite dyke running across the outcrop. These features are prominent in the fraction maps (a) and (c). Fraction map (b) shows the distribution of glacial till. All of these fraction maps correlate well with the geological maps of the area.

Section 2

This section covers the area containing mainly the phyllitic alteration, partially covered by overburden, as shown in fraction maps (g) and (f) respectively. These distributions correlate well with the known distributions over the site. Fraction map (f) shows the overburden lying mainly on the road crossing the site, as well as on the south eastern part of the outcrop. Fraction map (g) clearly shows the main phyllitic distribution along the central part of the site as well as some scattered reading along the south eastern part. These latter detections are weaker most likely because of the greater mixing occurring with the overburden signatures.

Section 3

This section was specifically analyzed to try to discriminate between graphitic/pyritic schist (both are present in combination) and overburden. Fraction map (d) shows the distribution of the graphitic and pyritic schist as obtained from the unmixing result.

Section 4

The detailed geological map shows a lamprophyre dyke cutting the mafic volcanic rock. Using the associated lab sample spectra, the linear unmixing model provided a distribution that correlates well with the known geometry of the dyke as shown in fraction map (e).

Non-Discriminated Alterations

Of the main constituent alterations mentioned above for the Marcus site, some discriminations were not well achieved. Bleached volcanic rocks were not well separated from overburden or phyllitic alterations. This may be because the rocks, even though classified as bleached by ground geologists, still contained enough phyllitic component to show up as such in the bandwidth studied. Another possible reason is that the outcrop area covered by very bleached rocks were not big enough to register over a pixel spatial size of about 5x5 m^2.

Phyllitic and propylitic alterations are two extremes, whereas the phyllitic altered rocks overprinted with propylitic are between these extremes in terms of chemical constituents [8]. For this reason, it was very

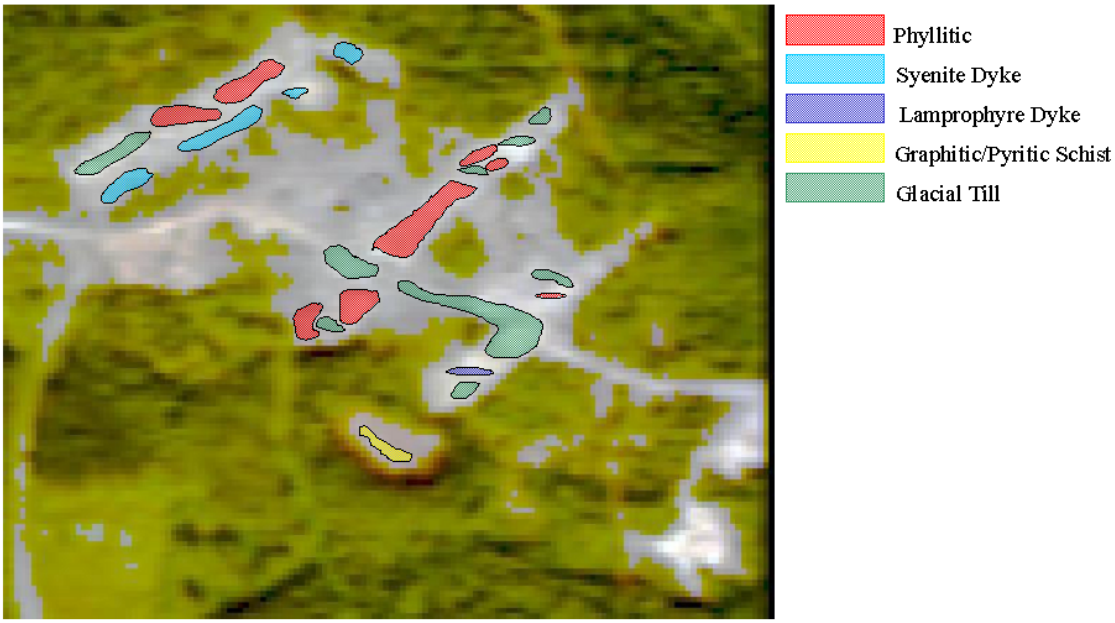

Figure 6. Qualitative map for the Marcus site showing the main features identified.

difficult to detect the two extremes and effectively discriminate between them since all three alterations are present across the site in mixtures. At the spatial resolution of this data, all three alterations were classed together as phyllitic.

Alteration Map

Figure 6 shows an extrapolated alteration map from the above results used for correlation with the detailed geological maps. Only the main features are shown for a qualitative assessment.

Conclusions

Several conclusions can be drawn from this work.

- The classification of propylitic and phyllitic alteration can be made on a sample level but was not distinguished at the resolution of the airborne data under the setting of the Marcus site. Both alteration fell within the tolerance level given to the phyllitic alterations and were classed as such.
- Bleached volcanic rocks were not distinguished from other units. This end-member either did not cover enough area in any pixel to be detected, and/or simply contained enough phyllitic characteristics at this resolution level to fall within the threshold of that class.
- Phyllitic alterations were well distinguished from the overburden and from the syenite dyke. These 3 units are well mapped.
- The lamprophyre occurences were distinguished from the phyllitic rocks.
- Graphitic/pyritic schist were also discriminated from the overburden.

The purpose of this initial analysis was to determine the potential of mapping the distribution of the end-members rather than quantifying the pixel content of each. More work needs to be done to better estimate the accuracy in quantifying the pixel content of each end-member.

It is not yet clear to what extent the correction process affected the results in this study. Each step of the correction may introduce new sources of noise and the cumulative process may be a factor in further limiting more detailed end-member discrimination. It is the intent of the authors to reprocess the raw data through the methodology presented here given these results in attempt to determine the influence of the processing steps on the outcome. Also, other sites around the Red Lake will be investigated in a similar manner to identify other types of alterations in the Greenstone belt and validate the repeatability of detecting these same units under different outcrop settings.

References

[1] Parker. J. R., "Gold Mineralization and Wall Rock Alteration in the Red Lake Greenstone Belt: A

Regional Perspective.", Summary of Field Work and other Activities; Ontario Geological Survey, Open File Report, 6032., 2000, pp 22-1 to 22-27.

[2] Folkman, M.A., DeLong, R.K., Willoughby, C.T., Gleichauf, D., Thordarson, S., Figueroa, M., and Procino, W., "TRWIS III: An Aircraft-Based Hyperspectral Imager", IRIS Passive Sensors Conference Proceedings, Environmental Research Institute of Michigan, March, 1996.

[3] Staenz, K., Szeredi, T., and Schwartz, J., "ISDAS – A System for Processing/Analyzing Hyperspectral Data." Canadian Journal of Journal of Remote Sensing, Vol.24, No.2, 1998, pp.99-113.

[4] Staenz, K., Neville, R.A., Clavette, S., Landry, R., and White, H.P., "Retrieval of Surface Reflectance from .Hyperion Radiance Data", 2002 International Geoscience and Remote Sensing Symposium, June, 2002, pp.1419-1421.

[5] Folkmann, M.A., Gleichauf, D.A., Willoughby, C.T., Thordarson, S., and Quon, B.H., "Performance Characterization and Calibration of the TRWIS III Hyperspectral Imager", Optical Science, Engineering, and Instrumentation Symposium, SPIE vol. 2819-15, August 1996.

[6] White, H.P., Miller, J.R., Chen, J.M., and Peddle, D.R., "Seasonal change in mean understorey reflectance for BOREAS sites: Preliminary Results", Proc. 17th Can. Symposium on Remote Sensing, 1995, pp.189-194.

[7] Richards, J.A., Xiuping, J., "Remote Sensing Digital Image Analysis.", Springer-Verlag, 1999, pp.334-335.

[8] C. Sasseville, personal communication, 2002.